Design Optimization Using Asymmetric Rotor in IPMSM for Torque Ripple Reduction Considering Forward and Reverse Directions

Jin-Cheol Park[1], Jae-Hyun Kim[1], Soo-Hwan Park[1,2], Ki-O Kim[1], Moo-Hyun Sung[3], and Myung-Seop Lim[1]

[1]Department of Automotive Engineering, Hanyang University, Seoul 04763, Republic of Korea
[2]Research and Development Division, Hyundai Motor Company, Hwaseong-si 18280, Republic of Korea
[3]Department of Automotive Engineering (Automotive-Computer Convergence), Hanyang University, Seoul 04763, Republic of Korea

In the interior permanent magnet synchronous motor (IPMSM), an asymmetric rotor is used as a design method to reduce torque ripple or cogging torque by adjusting the saturation of the rotor core. The advantage of an asymmetric rotor is that it can reduce torque ripple or cogging torque in the forward direction while maintaining the average torque or output power. However, when driving in the reverse direction, the torque ripple or cogging torque can be increased. Therefore, the asymmetric rotor produces different characteristics in the forward and reverse directions. In this study, the asymmetric rotor shape is designed using an optimization technique taking into consideration the rotating direction. The optimum design is performed based on the symmetric rotor as the base model. When rotating in the forward direction, the asymmetric rotor has a lower torque ripple than the symmetric rotor, and when rotating in the reverse direction, the asymmetric and symmetric rotors are designed to be similar. The kriging surrogate model was used to determine the optimum design point that satisfied the constraints. Finally, a symmetric and asymmetric rotor was manufactured and evaluated through tests.

***Index Terms*— Asymmetric rotor, electric vehicle (EV), interior permanent magnet synchronous motor (IPMSM), optimization, rotating direction, torque ripple.**

I. Introduction

THE advantage of an interior permanent magnet synchronous motor (IPMSM) is that it is known for having a high power density by utilizing the magnetic torque and the reluctance torque [1], [2], [3]. Accordingly, the IPMSM is used in various industrial components such as robots, electric vehicles (EVs), and home appliances to achieve high power density [4], [5], [6]. The industrial components using IPMSM are considered not only for high power density but also for low torque ripple as an important performance. The torque ripple is related to the noise and vibration characteristics of the IPMSM. Thus, it is necessary to reduce the torque ripple when designing an IPMSM. Many design methods have been studied for torque ripple reduction, such as rotor eccentricity, skew, notch, and chamfer [7], [8], [9], [10]. This method reduces torque ripple by designing the air-gap length by making the air-gap magnetic flux field distribution sinusoidal. However, the average torque decreases because the effective air-gap length increases [11]. A design method of asymmetric rotor shape has been proposed to reduce the torque ripple while maintaining the average torque [12]. The symmetric and asymmetric rotor shapes are illustrated in Fig. 1. Compared to the symmetric rotor shape, the asymmetric rotor shape can reduce the torque ripple without reducing the average torque while maintaining the air-gap length and adjusting the rotor core saturation by changing the permanent magnet (PM) position. The significant difference between the symmetric and asymmetric rotors is the effect of the rotating direction on the torque ripple. When applying a symmetric rotor in IPMSM, the torque ripple is constant regardless of the rotating directions. On the other hand, the torque ripple varies depending on the rotating directions when applying the asymmetric rotor in IPMSM. Some applications such as an EV traction motor require rotation in both the forward and reverse directions. In particular, the EV traction motor has a longer driving time in the forward direction than the driving time in the reverse direction. Therefore, it is necessary to consider the rotating direction in the design for reducing the torque ripple of the asymmetric rotor.

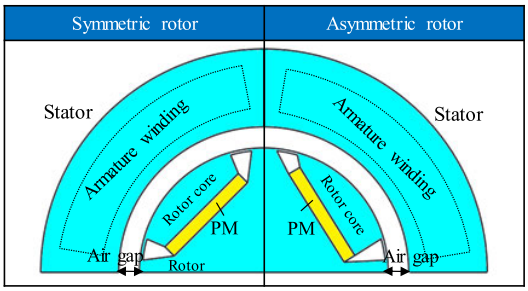

Fig. 1. Comparison between symmetric and asymmetric rotor shape.

In this article, the IPMSM with an asymmetric rotor shape is designed considering the rotating direction. Unlike the conventional method for the torque ripple reduction, the

Manuscript received 28 March 2023; revised 12 June 2023; accepted 27 June 2023. Date of publication 10 July 2023; date of current version 24 October 2023. Corresponding author: M.-S. Lim (e-mail: myungseop@hanyang.ac.kr).

Color versions of one or more figures in this article are available at https://doi.org/10.1109/TMAG.2023.3292295.

Digital Object Identifier 10.1109/TMAG.2023.3292295

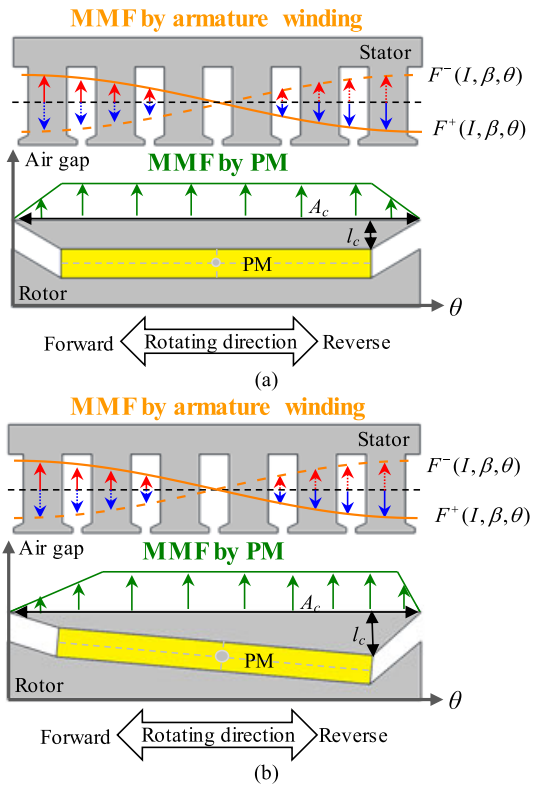

Fig. 2. MMF by armature winding and PM. (a) Symmetric rotor and (b) asymmetric rotor.

average torque is maintained with an asymmetric rotor. The base model is a symmetric rotor and the optimum model is an asymmetric rotor. Therefore, the torque ripple of the forward direction is minimized, and the torque ripple of the reverse direction is designed at the same level as the symmetric rotor. To verify the result of the design optimization, prototypes of the symmetric and the asymmetric rotor are fabricated and the experimental results of the symmetric and the asymmetric rotors are compared.

II. MMF for Comparison Between a Symmetric and an Asymmetric Rotor

Fig. 2 shows a schematic of the magnetic motive force (MMF) by the armature winding and PM. The MMF by the armature winding and PM is assumed to be linear. Also, the stator tooth and slot effect are ignored. The MMF by armature winding is assumed to be sinusoidal. The MMF is defined as

$$F = R\Phi \tag{1}$$

where F is the MMF, R is the magnetic reluctance, and Φ is the magnetic flux. The magnetic flux is determined based on magnetic reluctance. In an asymmetric rotor, the MMF by the PM can be determined by adjusting the permeability of the rotor core according to the position of the PM. The magnetic reluctance of the rotor core is expressed as

$$R_c = \frac{l_c(\theta)}{\mu_o \mu_r(\theta) A_c} \tag{2}$$

where R_c is the magnetic reluctance of the rotor core, μ_o is the vacuum permeability, μ_r is the relative permeability

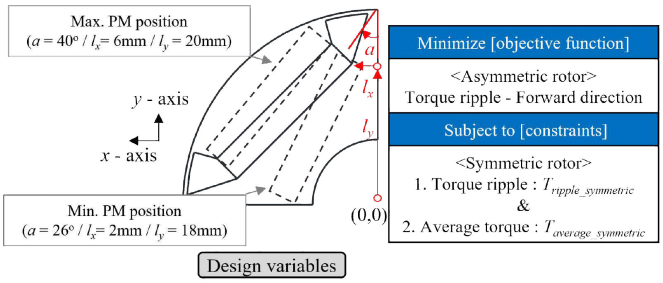

Fig. 3. Formulation for design optimization.

TABLE I
Specifications of Symmetric Rotor

Item	Unit	Value
Number of poles and slots	-	4 / 24
Stator diameter	mm	86
Stack length	mm	45
PM type	-	N45SH
DC link voltage	V	48
Rated input current	A_{rms}	60

of the material, l_c is the distance between the rotor diameter and PM, and A_c is the cross-sectional area of the rotor core. In a symmetric rotor, the MMF by the PM is generated symmetrically. However, the area of the rotor core in the asymmetric rotor is not constant depending on the rotor position. As the distance between the rotor diameter and PM is shortened, the permeability and magnetic reluctance of the rotor core increase. Therefore, the MMF by PM is generated asymmetrically.

The rotating direction is determined by the amplitude and angle of the MMF by the armature winding. If the MMF by the armature winding is positive, the rotor rotates in the forward direction. The positive MMF by the armature winding is expressed as

$$F_a(I,\beta,\theta)^+ = \frac{3\sqrt{2}\, k_w N I}{p}\cos(p\theta+\beta) \tag{3}$$

where F_a is the MMF by the armature winding, I is the armature current, β is the armature current angle, θ is the electrical angle, k_w is the winding factor, N is the number of series turns per phase, and p is the pole pair. If the MMF by armature winding is negative, the rotor rotates in the reverse direction. The negative MMF by the armature winding is expressed as

$$F_a(I,\beta,\theta)^- = -\frac{3\sqrt{2}\, k_w N I}{p}\cos(p\theta+\beta). \tag{4}$$

The torque and torque ripple are generated by the interaction of the MMF by the armature and PM. In the symmetric rotor, the torque ripple is the same regardless of the rotating direction. However, In the asymmetric rotor, torque ripple occurs differently depending on the rotating direction.

III. Design Optimization for an Asymmetric Rotor

The symmetric rotor is used as the base model to perform the optimum design. The specifications of the symmetric rotor

TABLE II
BOUNDARIES OF DESIGN VARIABLES

Design variables	Unit	Min.	Max.
Positional angle of PM (a)	°	26	40
x-axis directional displacement (l_x)	mm	2	6
y-axis directional displacement (l_y)	mm	18	20

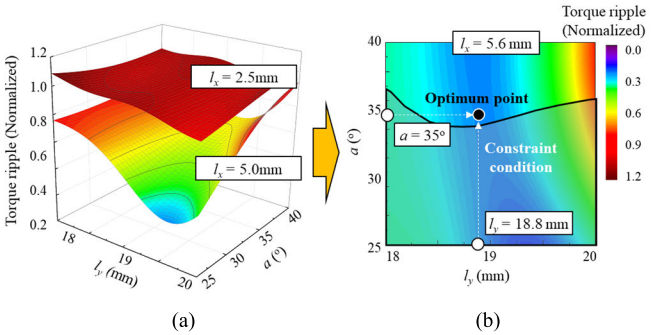

Fig. 4. Constructed (a) kriging surrogate model and (b) part of the kriging surrogate model for determining optimum point.

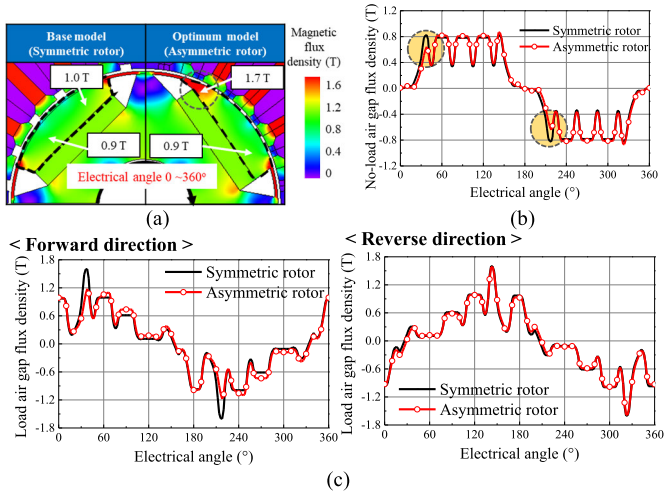

Fig. 5. Optimum design result (a) no-load core saturation, (b) no-load air-gap flux density, and (c) load air-gap flux density according to rotating direction.

are summarized in Table I. For comparison, the same stator of the symmetric rotor was used in the asymmetric rotor design. Moreover, the PM size, pole angle, rib thickness, and rib angles were the same as those of the symmetric rotor. By applying the asymmetric rotor, the air-gap magnetic field distribution under load conditions can be sinusoidal compared to the symmetric rotor. Considering that the magnetic permeance of the rotor is determined by the rotor shape, the three design variables are selected as shown in Fig. 3. In the figure, the l_x and l_y represent the x-axis and y-axis directional displacements, respectively. a represents the positional angle of the PM. The maximum and minimum ranges of the design variables summarized in Table II are determined by confirming the magnet position to be located within the outer and inner rotor diameter according to the design variables. The objective function and the constraints for the torque ripple minimization are defined considering the forward and reverse directions. The objective function and constraint condition are used to determine the optimum design point from the kriging surrogate model. They are expressed as

$$\begin{aligned} &\min\ F(\mathbf{x}) = y_1(\mathbf{x}) \\ &\text{s.t. } G_1(\mathbf{x}) = y_2(\mathbf{x}) \le T_{\text{average\_symmetric}} \\ &\qquad G_2(\mathbf{x}) = y_3(\mathbf{x}) \le T_{\text{ripple\_symmetric}} \end{aligned} \tag{5}$$

where $\mathbf{x}$ is the vector of the design variables, F is the objective function, G is the constraint condition, y_1 is the torque ripple of the asymmetric rotor in the forward direction, y_2 is the average torque of the asymmetric rotor, and y_3 is the torque ripple of the asymmetric rotor in the reverse direction.Because the targeted system mainly rotates in the forward direction, the torque ripple when rotating in the forward direction is set as the objective function while the torque ripple when rotating in the reverse direction is considered in the constraints. In addition, the average torque was maintained with the value of the base model.

The surrogate model was used to predict the torque ripple for the optimum model. Kriging was used as the interpolation method for the data in the surrogate model. This technique is widely used in the design optimization of electric motors [13]. A combination of optimal Latin hypercube design (OLHD) and sequential maximin distance design (SMDD) is applied as a design of experiment (DOE) to create the kriging surrogate model [14]. The number of sample points was selected as 50 through the DOE. The kriging surrogate model was constructed as shown in Fig. 4(a). The kriging surrogate model is required for verification using the leave-one-out cross-validation method [15]. The normalized root mean square error (NRMSE) of the kriging surrogate model is expressed as

$$\text{NRMSE} = \sqrt{\frac{1}{n_s}\cdot\sum_{i=1}^{n_s}\left(\frac{Y(x_i)-\hat{Y}^{(-i)}(x_i)}{\max\{\mathbf{Y}(\mathbf{x})\}-\min\{\mathbf{Y}(\mathbf{x})\}}\right)^2}\cdot 100\% \tag{6}$$

where n_s is the number of sample points, $\mathbf{Y}(\mathbf{x})$ is the vector of the response values, which can be the torque ripple in the torque ripple in the forward direction. $Y(x_i)$ is the response at the ith point calculated from the finite element analysis (FEA) simulation. $\hat{Y}^{(-i)}(x_i)$ is the predicted response at the ith point calculated from the kriging surrogate model. The NRMSE for the torque ripple in the forward was calculated at 5.2%. The results were considered sufficiently accurate. The optimum design point is satisfied with both the objective function and constraint condition from the kriging surrogate model. As part of the kriging surrogate model, Fig. 4(b) shows the results of the torque ripple in the forward direction according to the a and l_y with l_x at 5.6 mm. The optimum design point is selected as the point with the smallest torque ripple in the forward direction while satisfying the constraint condition.

Fig. 5 shows the symmetric rotor shape and the asymmetric rotor shape determined by the optimum design. Also, the no-load and load air-gap flux density using FEA simulation are summarized. Fig. 5(a) shows the no-load core saturation of symmetric and asymmetric rotors. It was confirmed that the permeability distribution of the rotor core differed within the same no-load condition. Fig. 5(b) shows the no-load air-gap flux density of symmetric and asymmetric rotors. In an

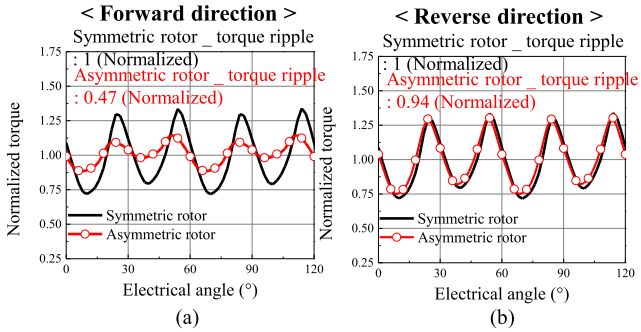

Fig. 6. Simulation result of torque ripple (a) forward direction and (b) reverse direction.

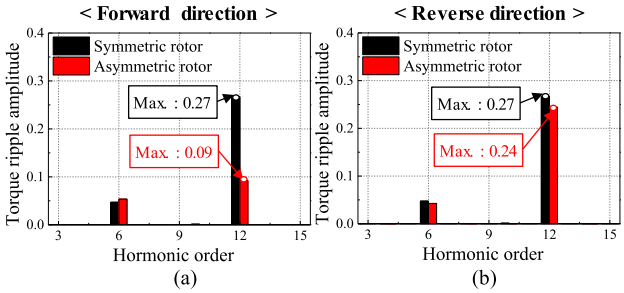

Fig. 7. Harmonic analysis for simulation result of torque ripple (a) forward direction and (b) reverse direction.

asymmetric rotor, the air-gap flux density decreases in the high saturation region of the rotor core. Fig. 5(c) shows the load air-gap flux density according to the rotating direction. The simulation was conducted under the same input current at 60 A_{rms} and the current angle at 30°. In the case of the forward direction, lower harmonics of the air-gap flux density are generated for an asymmetric rotor than for a symmetric rotor. Fig. 6 shows the simulation results for the torque waveform according to the rotating direction of the symmetric and asymmetric rotors. When the motor is operated in the forward direction, the torque ripple of the asymmetric rotor is reduced by about 53% rather than the symmetric rotor. When the motor is operated in the reverse direction, the torque ripple of the symmetric and asymmetric rotor is similar. Fig. 7 shows the harmonic analysis of the torque waveform. In the forward direction, the torque ripple and the 12th component of the asymmetric rotor are reduced. In the reverse direction, it was confirmed that the symmetric and asymmetric rotors generated the same torque ripple.

IV. Validation

Fig. 8 shows the manufactured symmetric and asymmetric rotor. The asymmetric rotor is manufactured based on the PM position determined by the optimum design. Also, the same iron core and shaft materials are used for the symmetrical and asymmetrical rotors. Fig. 9 shows the experimental setup for the no-load and load test which were performed to evaluate the torque ripple for the manufactured symmetric and asymmetric rotors. The back electromagnetic force (EMF) was measured through a no-load test. Through the load test, the torque ripple was evaluated using a torque sensor under the same applied current, phase angle, and voltage.

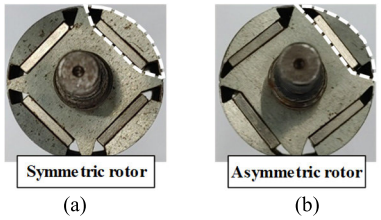

Fig. 8. Manufactured rotor shape (a) symmetric rotor and (b) asymmetric rotor.

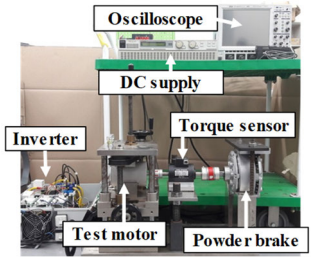

Fig. 9. Experimental setup.

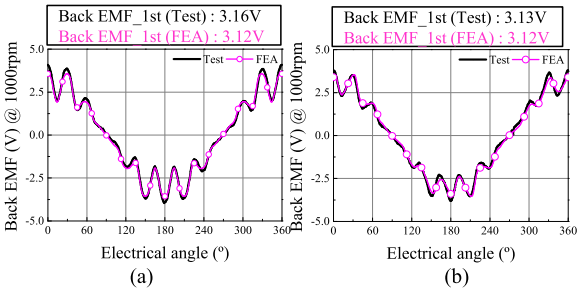

Fig. 10. Comparison of back EMF test and simulation result (a) symmetric rotor and (b) asymmetric rotor.

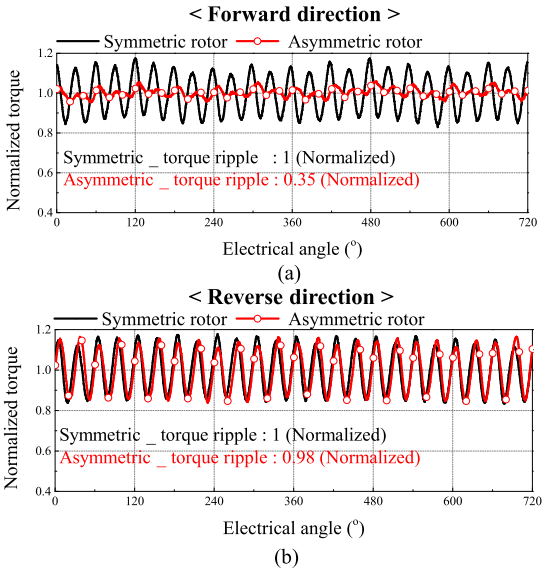

Fig. 11. Test result of torque (a) forward direction and (b) reverse direction.

Fig. 10 shows the back EMF of the test and simulation result. It was confirmed that the simulation and test results were similar under the same rotor speed at 1000 r/min. The torque ripple of the symmetric and asymmetric rotors was confirmed through the load test. Fig. 11 summarizes the torque ripple test results for the symmetric and asymmetric

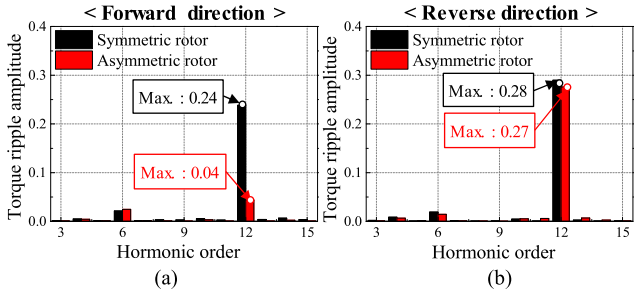

Fig. 12. Harmonic analysis for test result of torque ripple (a) forward direction and (b) reverse direction.

rotors. The torque ripple test was conducted under the same input current at 60 A_{rms} and the current angle at 30°. In the forward direction, the torque ripple for the asymmetric rotor is reduced to about 65% compared to the symmetric rotor. In the reverse direction, the difference in torque ripple between the symmetric and asymmetric rotors is approximately 2%. Fig. 12 shows the results of the harmonic analysis for torque ripple. In particular, it can be seen that the torque ripple of the 12th component is reduced. In the forward direction, the torque ripple is lower in the asymmetric rotor than in the symmetric rotor. In the reverse direction, the harmonic order and amplitude of torque ripple are similar for both the symmetric and the asymmetric rotors.

V. Conclusion

In this article, a design method using an asymmetric rotor was proposed for torque ripple reduction considering the forward and reverse directions. The torque ripple in the reverse direction and the average torque are similar to those of the symmetric rotor, while the torque ripple in the forward direction is reduced. Therefore, the design results can be implemented in various applications with the forward and reverse rotations of the asymmetric rotor.

References

[1] H.-J. Kim and C.-S. Lee, "Shape parameters design for improving energy efficiency of IPM traction motor for EV," *IEEE Trans. Veh. Technol.*, vol. 70, no. 7, pp. 6662–6673, Jul. 2021.

[2] T.-A. Huynh, P.-H. Chen, and M.-F. Hsieh, "Analysis and comparison of operational characteristics of electric vehicle traction units combining two different types of motors," *IEEE Trans. Veh. Technol.*, vol. 71, no. 6, pp. 5727–5742, Jun. 2022.

[3] J.-C. Son, J.-Y. Kim, J.-W. Choi, D.-K. Lim, and H.-K. Yeo, "Performance enhancement of the IPMSM for HEV applications using grain-oriented electrical steel and design optimization," *IEEE Access*, vol. 10, pp. 46599–46607, 2022.

[4] Y. Shimizu, S. Morimoto, M. Sanada, and Y. Inoue, "Investigation of rotor topologies for reducing torque ripple in double-layer IPMSMs for automotive applications," *IEEE Trans. Ind. Electron.*, vol. 70, no. 8, pp. 8276–8285, Aug. 2023.

[5] H.-S. Jung, H. Kim, S.-K. Sul, and D. J. Berry, "Permanent magnet temperature estimation in a mass-produced traction motor for an electric vehicle," *IEEE Trans. Transport. Electrific.*, vol. 8, no. 2, pp. 1863–1873, Jun. 2022.

[6] T. Zou et al., "A comprehensive design guideline of hairpin windings for high power density electric vehicle traction motors," *IEEE Trans. Transport. Electrific.*, vol. 8, no. 3, pp. 3578–3593, Sep. 2022.

[7] S.-I. Kim, J.-Y. Lee, Y.-K. Kim, J.-P. Hong, Y. Hur, and Y.-H. Jung, "Optimization for reduction of torque ripple in interior permanent magnet motor by using the Taguchi method," *IEEE Trans. Magn.*, vol. 41, no. 5, pp. 1796–1799, May 2005.

[8] W. Q. Chu and Z. Q. Zhu, "Investigation of torque ripples in permanent magnet synchronous machines with skewing," *IEEE Trans. Magn.*, vol. 49, no. 3, pp. 1211–1220, Mar. 2013.

[9] X. Ge, Z. Q. Zhu, G. Kemp, D. Moule, and C. Williams, "Optimal step-skew methods for cogging torque reduction accounting for three-dimensional effect of interior permanent magnet machines," *IEEE Trans. Energy Convers.*, vol. 32, no. 1, pp. 222–232, Mar. 2017.

[10] G.-H. Kang, Y.-D. Son, G.-T. Kim, and J. Hur, "A novel cogging torque reduction method for interior-type permanent-magnet motor," *IEEE Trans. Ind. Appl.*, vol. 45, no. 1, pp. 161–167, Feb. 2009.

[11] Y.-H. Jung, M.-S. Lim, M.-H. Yoon, J.-S. Jeong, and J.-P. Hong, "Torque ripple reduction of IPMSM applying asymmetric rotor shape under certain load condition," *IEEE Trans. Energy Convers.*, vol. 33, no. 1, pp. 333–340, Mar. 2018.

[12] W. Ren, Q. Xu, Q. Li, and L. Zhou, "Reduction of cogging torque and torque ripple in interior PM machines with asymmetrical V-type rotor design," *IEEE Trans. Magn.*, vol. 52, no. 7, pp. 1–5, Jul. 2016.

[13] S. Kim, S.-G. Lee, J.-M. Kim, T. H. Lee, and M.-S. Lim, "Robust design optimization of surface-mounted permanent magnet synchronous motor using uncertainty characterization by bootstrap method," *IEEE Trans. Energy Convers.*, vol. 35, no. 4, pp. 2056–2065, Dec. 2020.

[14] S. Kim, S. Lee, J. Kim, T. H. Lee, and M. Lim, "Uncertainty identification method using kriging surrogate model and Akaike information criterion for industrial electromagnetic device," *IET Sci., Meas. Technol.*, vol. 14, no. 3, pp. 250–258, May 2020.

[15] N. V. Queipo, R. T. Haftka, W. Shyy, T. Goel, R. Vaidyanathan, and P. K. Tucker, "Surrogate-based analysis and optimization," *Prog. Aerosp. Sci.*, vol. 41, no. 1, pp. 1–28, Jan. 2005.